JOURNAL OF GEOPHYSICAL RESEARCH: SPACE PHYSICS, VOL. 118, 4093–4107, doi:10.1002/jgra.50388, 2013

Comparison of high-altitude production and ionospheric outflow contributions to O^+ loss at Mars

Michael W. Liemohn,[1] Shannon M. Curry,[1] Xiaohua Fang,[2] and Yingjuan Ma[3]

Received 18 March 2013; revised 16 May 2013; accepted 4 June 2013; published 8 July 2013.

[1] The Mars Test Particle model is used (with background parameters from a magnetohydrodynamic code) to simulate the transport of O^+ ions in the near-Mars space environment to study the source processes responsible for ion escape. The MHD values at this altitude are used to inject an ionospheric outflow source of ions for the Mars Test Particle (MTP). The resulting loss distributions (in both real and velocity space) from this ionospheric source term are compared against those from high-altitude ionization mechanisms, in particular photoionization, charge exchange, and electron impact ionization, each of which has its own source regions, albeit overlapping. For the nominal MHD settings, this ionospheric outflow source contributes only 10% to the total O^+ loss rate at solar maximum, predominantly via the central tail region. This percentage has very little dependence on the initial temperature, but a change in the initial ion density or bulk velocity directly alters this loss through the central tail. A density or bulk velocity increase of a factor of 10 makes the ionospheric outflow loss comparable in magnitude to the loss from the combined high-altitude sources. The spatial and velocity space distributions of escaping O^+ are examined and compared for the various source terms to identify features specific to each ion source mechanism. For solar minimum conditions, the nominal MHD ionospheric outflow settings yield a 27% contribution to the total O^+ loss rate, i.e., roughly equal to any one of the three high-altitude source terms with respect to escape.

Citation: Liemohn, M. W., S. M. Curry, X. Fang, and Y. Ma (2013), Comparison of high-altitude production and ionospheric outflow contributions to O^+ loss at Mars, *J. Geophys. Res. Space Physics*, *118*, 4093–4107, doi:10.1002/jgra.50388.

1. Introduction

[2] Several processes are known to contribute to the loss of planetary ions from the Mars upper atmosphere, in particular for O^+ but also the heavier molecular ion species of CO_2^+ and O_2^+. Some studies discuss the flow of ions from the ionosphere proper (i.e., altitudes below 250 km) as the main loss process for oxygen ions from Mars [e.g., *Lundin et al*., 2006b; *Brecht and Ledvina*, 2012], sometimes purely from the dynamical flow patterns in the transition region between the ionosphere and solar wind magnetosheath above it [e.g., *Lundin et al*., 2004; *Penz et al*., 2004; *Brecht and Ledvina*, 2006; *Barabash et al*., 2007; *Perez-de-Tejada et al*., 2009; *Kallio et al*., 2010] but also in the context of localized acceleration mechanisms like wave heating [*Lundin et al*., 2006b; *Ergun et al*., 2006; *Andersson et al*., 2010], parallel electric fields [e.g., *Boesswetter et al*., 2004; *Brain et al*., 2006; *Lundin et al*., 2006a; *Dubinin et al*., 2009], or magnetic reconnection [e.g., *Liemohn et al*., 2006, 2007; *Eastwood et al*., 2008; *Harnett*, 2009; *Brain et al*., 2010b].

[3] While some observational studies of the escape of O^+ from Mars are careful to simply refer to high-altitude O^+ as a planetary ion [e.g., *Verigin et al*., 1991; *Fedorov et al*., 2006], many studies often use the term ionospheric outflow for the source of the particles measured far from the planet. *Lundin et al*. [2008, 2009] used this term for the Mars Express observations of planetary ions observed at high altitude but within the induced magnetospheric boundary (i.e., in the tail behind the planet). This is similar to the finding from Phobos-2 observations of planetary ions in the tail region [e.g., *Lundin et al*., 1989, 1990; *Kallio et al*., 1994]. However, several studies from the Phobos-2 mission data set revealed high-energy (greater than 50 keV) O^+ ions [*Afonin et al*., 1989; *Kirsch et al*., 1991; *McKenna-Lawler et al*., 1993, 2012], presumably coming from ionization of the high-altitude exosphere [*Cravens et al*., 2002]. Similarly, *Carlsson et al*. [2006] noted that the escape rate of planetary ions is more than the ionosphere can typically supply, indicating that either there are additional acceleration processes in the topside ionosphere or that there is a significant high-altitude source.

[4] Modeling studies, like *Brain et al*. [2010a] (and references to the many modeling studies therein), regularly refer to any planetary ion as "ionospheric" in origin, regardless of the altitude of ionization. This is convenient from a

[1]Department of Atmospheric, Oceanic, and Space Sciences, University of Michigan, Ann Arbor, Michigan, USA.
[2]Laboratory for Atmospheric and Space Physics, University of Colorado Boulder, Boulder, Colorado, USA.
[3]Institute for Geophysics and Planetary Physics, University of California, Los Angeles, California, USA.

Corresponding author: M. W. Liemohn, University of Michigan, 2455 Hayward St., Ann Arbor, MI 48109-2143, USA. (liemohn@umich.edu)

2169-9380/13/10.1002/jgra.50388

variable naming standpoint within numerical models: solar wind ions are those that come into the simulation domain through the outer boundary, while ionospheric ions are those entering through the inner boundary or produced within the simulation domain. The problem with this word usage is that the typical use of the term "ionosphere" refers only to the highly conducting layer of peak ionization coincident with the planet's thermosphere. For Mars, this is the altitude range from 100 km to perhaps 250 km altitude [e.g., *Brecht*, 1997; *Boesswetter et al*., 2004; *Ma et al*., 2004; *Brecht and Ledvina*, 2010]. Further confusion arises because some modeling studies use the term "ionospheric loss" even when the model inner boundary is above the nominal ionosphere [e.g., *Kallio and Janhunen*, 2002; *Modolo et al*., 2005; *Harnett and Winglee*, 2006]. Other modeling studies have shown, however, that the source region for escaping ions is above the ionosphere, resulting from ionization of the neutral exosphere within the magnetosheath [e.g., *Luhmann*, 1990; *Cravens et al*., 2002; *Curry et al*., 2013a]. These later studies find that majority of the escaping O^+ ions are produced above 300 km altitude.

[5] *Ma et al*. [2004] briefly commented on the issue of the source altitude for escaping O^+ ions. They calculated the total fluence through various altitude shells within their multispecies magnetohydrodynamic (MHD) modeling results, determining that the fluence saturated in the 350–450 km altitude range (note that the lower boundary in that simulation was 100 km altitude). However, they did not investigate the ionization processes and transport mechanisms of the ions dominating the total escape rate. Therefore, it was left ambiguous whether the escape was dominated by ionospheric outflow or by ionization processes at higher altitudes.

[6] Using a test particle model through the electric and magnetic fields of the *Ma et al*. [2004] simulation results, *Fang et al*. [2010b] conducted a rigorous quantification of the percentage of O^+ ions escaping to deep space as a function of their altitude of ionization. It was determined that the fraction of ions that escape among those produced at a given altitude is below 10–20% at 200 km (depending on solar wind conditions and the local time of the crustal fields), and that this fraction did not cross the 50% mark until an altitude of 400–500 km. The escape fractions reached a saturation value of 70–90% above 600 km, with some ions of high-altitude origin being directed toward the planet by the solar wind convective electric field, resulting in bombardment of the upper atmosphere [cf. *Luhmann and Kozyra*, 1991; *Johnson*, 1994; *Kallio and Koskinen*, 1999; *Fang et al*., 2013].

[7] Similarly, *Fang et al*. [2010a] directly compared ionospheric outflow with high-altitude ionization processes, concluding that the fluid-like flow of O^+ from low altitudes (below 200 km altitude) to deep space is negligible. This study, however, used the background MHD quantities for the ionospheric outflow initialization parameters. Furthermore, the ionospheric outflow test particles were launched from the inner boundary. This is problematic because the particles will gyrate around the local magnetic field, and nearly all will cross the plane of the inner boundary on their first cycle. Therefore, the role of ionospheric outflow could have been underestimated in the *Fang et al*. [2010a] study.

[8] In the work presented below, the contribution of ionospheric outflow to the escaping flux of O^+ from Mars is investigated. Similar to *Modolo et al*. [2005], the ionospheric outflow is incorporated by injecting particles at a given altitude using the MHD plasma values at that location. In addition, the ionospheric outflow initialization parameters are systematically varied to determine the influence of each of these factors on the relative contribution of ionospheric outflow to the total loss rate. Understanding the origin of escaping O^+ addresses one of the many variables in the larger question of atmospheric erosion and evolution.

2. Model

[9] The Mars Test Particle (MTP) model will be used for this study for the transport of O^+ through the Mars space environment. Originally unveiled by *Fang et al*. [2008], *Curry et al*. [2013a] recently modified this numerical tool by including several different functional forms for the pickup ion source processes. Briefly, the MTP code launches the particles, which represent the planetary O^+ ions in near-Mars space, with weighting terms set according to these source term ionization rates and then calculates their motion through near-Mars space using a background electric and magnetic field description from a different model calculation. In this study, the background field is that from the multispecies magnetohydrodynamic (MHD) calculations of *Ma et al*. [2004]. The inner boundary of the model is set to 300 km altitude, and the outer boundary is placed at 4 R_M planet-centric distance. Note that a similar test particle modeling procedure through this same MHD model was recently developed by *Li and Zhang* [2009].

[10] The simulation volume is divided into ~300,000 "source cells" (107 radial × 36 polar × 72 azimuthal), and then 5000 test particles are launched from within each of these cells. Each particle is proportionately weighted with the local ionization rate from each of the three processes: photoionization, charge exchange, and electron impact ionization. The particles are then randomly assigned a starting location within the cell and randomly assigned a velocity based on a Maxwellian distribution around the local neutral oxygen temperature. Therefore, roughly 1.4 billion particles are launched for these high-altitude source terms in order to resolve the fine-scale features of the high-altitude velocity space distributions of the escaping ions [cf. *Curry et al*., 2013a, 2013b].

[11] The high-altitude pickup ion source terms are those of the "baseline" case from *Curry et al*. [2013a]. Photoionization is taken to be a constant rate everywhere in the simulation domain except in the optical shadow of the planet, the charge exchange reaction rate is set proportional to the total velocity (bulk plus thermal) of the solar wind H^+ from the MHD results, and electron impact ionization uses the *Cravens et al*. [1987] temperature dependent reaction rates.

[12] For this study, a fourth source term has been added to the calculation: ionospheric outflow (IO). This is defined from the local MHD flux at a selected altitude shell close to the inner boundary of the MTP simulation domain. Launching these particles from the exact surface of the inner MTP boundary creates unrealistically low escape rates from this process. This is because many particles launched precisely from the lower boundary will gyrate once and then

strike the inner boundary, thus being "lost" from the MTP simulation domain. This will happen even for particles with an upward drift speed if the magnetic field is oblique and/or the thermal speed is higher than the drift speed. To work around this numerical obstacle, the IO particles are launched within a source term spatial grid cell above the altitude shell at which the MHD flux values are selected (i.e., for this study, between 300 and 337 km altitude). By multiplying the flux by the cell face area, an effective "ionization rate" in units of ions/s is obtained. This rate is exactly analogous to the high-altitude pickup ion source term rates, and the same volumetric random launch scenario can be applied. The only difference is that the initial velocity of the particles is based on the local MHD temperature, with an additional initial velocity component from the local MHD bulk flow vector.

[13] Note that these IO particles are different from the three "high-altitude source" particles launched by the MTP simulation. The other particles are given a proportional weight for the three sources (photoionization, charge exchange, and electron impact), while the IO particles are given only the weighting of the outflow source. The high-altitude sources could be combined into the same particle set because the initial conditions were the same within each source cell (only the weighting is different). The IO source, however, has a different temperature (the local plasma temperature, not the neutral temperature) and is given an initial bulk velocity (with all of the particles in a cell receiving the MHD bulk velocity as well as a randomly determined velocity based on a Maxwellian distribution). In addition, because the IO source is launched at only one altitude shell, the number of particles per cell is set to 100 times that for the other sources (which are launched in roughly 100 times more source cells) in order to achieve adequate resolution in the high-altitude velocity space distributions. Therefore, the total number of test particles is roughly the same (~1.3 billion particles) for ionospheric outflow as for the high-altitude source terms. That is, a total of ~2.7 billion particles are launched for each simulation.

[14] The MHD simulations used for the background fields solve separate continuity equations for four ion species but a single set of momentum and energy equations. It takes into account the effect of the crustal magnetic field with the *Arkani-Hamed* [2001, 2002] Mars crustal field model and uses thermospheric neutral densities from *Bougher et al.* [2000]. The upstream boundary conditions are set to a solar wind density of 4 cm^{-3}, velocity of 400 km/s, and a nominal away-sector Parker spiral interplanetary magnetic field (IMF) of 3 nT with an angle of 56° off of the x axis (of Mars solar orbital coordinates).

[15] The MHD inputs used for the injected ionospheric outflow at 300 km altitude are given in Figure 1. On the dayside, the O^+ density (Figure 1a) is near 1000 cm^{-3}, but it plunges to values below 100 cm^{-3} (even below 1 cm^{-3}) across the nightside. The bulk velocity (Figure 1b) is small across most of the dayside (below 100 m/s) and is only slightly higher on average across the nightside (still below 1 km/s) except in one location, on the nightside at high southern latitudes. Viewed from upstream, this is a region directly behind the strong crustal fields, and the flow (of tens of km/s) is downward. Note that the bulk speed from the MHD results is applied regardless of direction. This allows for downward or nearly horizontally flowing O^+ to be included in the IO boundary condition. Such particles might escape, depending on the local and downstream magnetic and electric field vectors. Even if the bulk flow is downward, the temperature could be large compared to the bulk flow, and some particles would be directed upward. Therefore, ionospheric outflow is initialized everywhere on the source shell, regardless of the direction of the bulk flow vector. In Figure 1c, it is seen that the boundary condition has dayside temperatures ranging from a few hundred Kelvin in the Northern Hemisphere to a few thousand Kelvin in the Southern Hemisphere over the region of strong crustal fields. The temperatures are higher on the nightside, reaching ~5000 K across most of the nightside; and in the region of downwelling flow in the southern high latitude nightside, the temperature is over 10^5 K. Figure 1d shows the initial

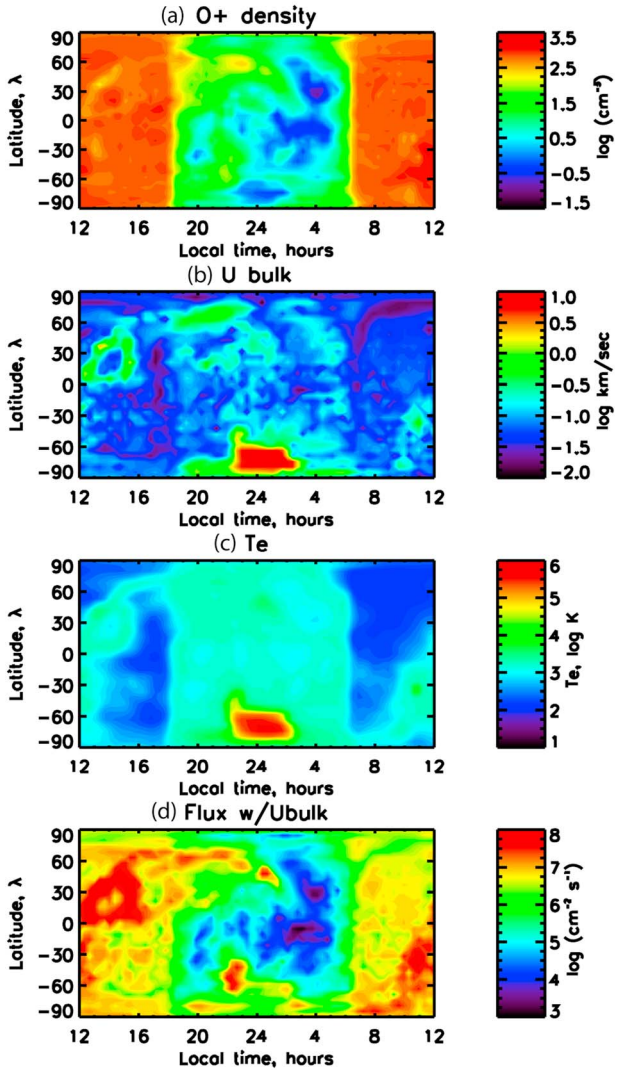

Figure 1. MTP ionospheric outflow boundary conditions taken at 300 km altitude in the MHD model results: (a) O^+ density; (b) bulk velocity; (c) temperature; and (d) O^+ flux. Each plot has local time as the x axis (noon on the ends, midnight in the middle) and latitude as the y axis (poles at the top and bottom, equator in the middle), with its own logarithmic color scale.

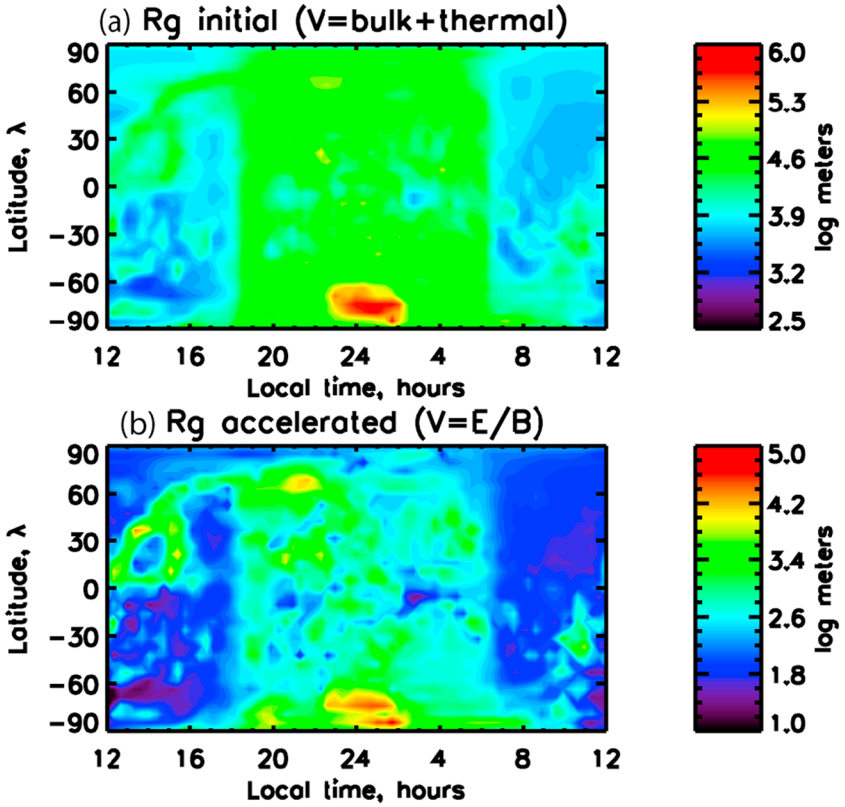

Figure 2. Local O^+ gyroradius at 300 km altitude from the MHD model results, with the assumed velocity from (a) the local speed calculated from the bulk and thermal velocities, and (b) the local pick-up acceleration flow from the electric and magnetic field strengths. Each plot has local time as the *x* axis (noon on the ends, midnight in the middle) and latitude as the *y* axis (poles at the top and bottom, equator in the middle), with its own logarithmic color scale.

condition fluxes used for weighting the MTP IO ions. The largest fluxes (~10^8 cm^{-2} s^{-1}) are found in a few places on the dayside, with much smaller fluxes across the nightside. Integrated over the entire shell, the O^+ ionospheric outflow "production rate" is 1.9×10^{25} ions s^{-1}.

[16] Before proceeding, the chosen methodology should be tested. Specifically, it is useful to check the O^+ gyroradius at the MTP inner boundary. Two calculations of this quantity are shown in Figure 2: Figure 2a is a gyroradius calculation based on the MHD bulk speed and characteristic "random" speed from the local temperature value; and Figure 2b is the gyroradius calculation with the velocity set to the "pickup E/B" velocity. Because the first MTP source grid cell has a vertical extent of 37 km, the average launch altitude of the IO test particles is 19 km above the MTP simulation's domain inner boundary. In general, the gyroradius calculated from the initial conditions (Figure 2a) is higher than those from pickup acceleration (Figure 2b). This is because 300 km is within the magnetic pileup region (or dominated by the strong crustal fields), and the flow speed is rather low, therefore the pickup acceleration at this altitude is small. Across the dayside, the gyroradius is below 10 km nearly everywhere. On the nightside, the gyroradius is larger, typically between 10 and 100 km, and in fact goes above 1000 km in the small region of downwelling at high southern latitudes. Note from Figure 1 that the largest IO fluxes are on the dayside. From this, it is concluded that the assumption of launching particles at a distributed altitude source throughout the first MTP grid cell is a reasonable approach that essentially avoids the problem of particles striking the inner boundary after their first gyration.

3. Results

[17] The presentation of the results begins with an examination of the fine-scale structure in the velocity space distributions of the escaping ionospheric outflow, then progresses to spatial distributions of the escaping particles, and finally to total escape rates. A discussion of the interpretation and implications of these results is given in the following section.

3.1. Velocity Space Distributions

[18] Figure 3 shows flight direction distributions at 3.9 R_M Mars-centric distance (i.e., just inside the outer boundary of the simulation domain) at two locations: (Figures 3a and 3b) along the *x* axis in the central downtail direction and (Figures 3c and 3d) over the northern pole in the direction of the +Z MSE (Mars-Sun-Electric field coordinate system) axis. Figures 3a and 3c show the results for the ionospheric outflow, and Figures 3b and 3d show the sum of the three high-altitude source terms (photoionization, charge exchange, and electron impact ionization). The fluxes are integrated over energy. Here flight direction refers to the

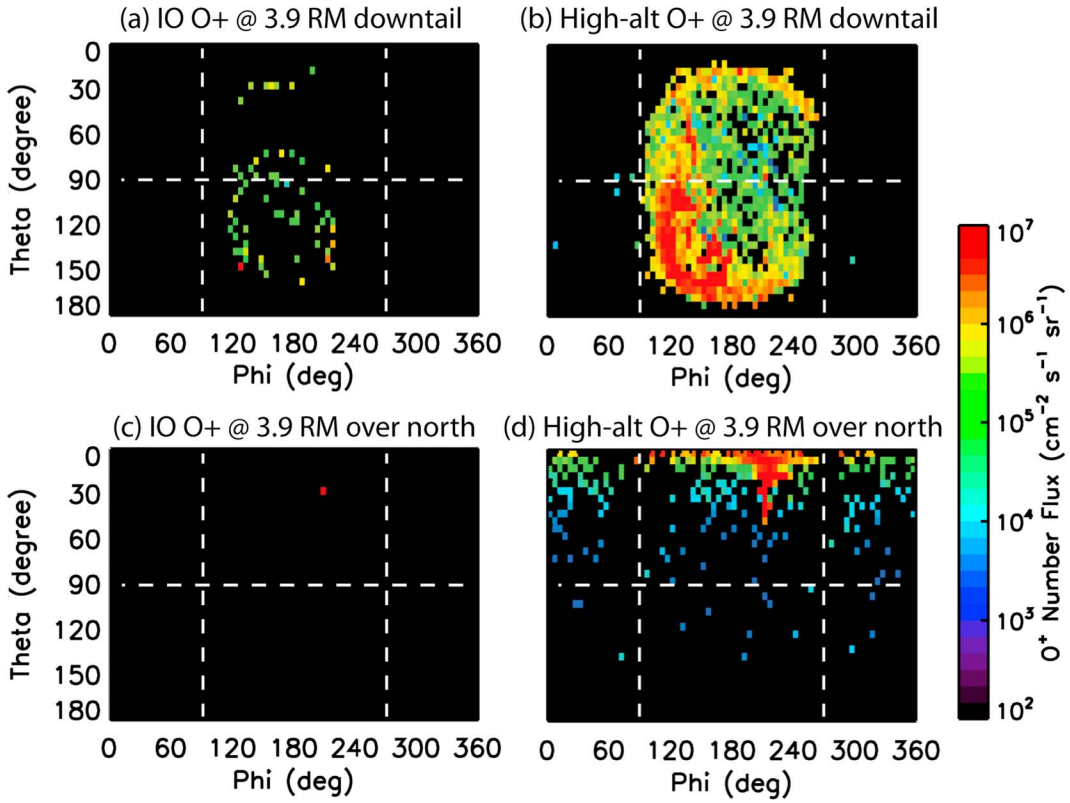

Figure 3. O^+ velocity space (flight direction) distributions at 3.9 R_M (a and b) Mars-centric distance in the $-X_{MSE}$ downtail direction and (c and d) over the north pole in the $+Z_{MSE}$ direction for the IO source term (Figures 3a and 3c) and for the three high-altitude source terms combined (Figures 3b and 3d). The plots, summed over all particle energies, show a resolution of $5° \times 5°$ with the azimuthal angle on the x axis (sunward flow on the edges, tailward flow in the middle) and polar angle on the y axis (northward motion on the upper half, southward motion on the lower half), all on the same logarithmic color scale.

polar angle (θ) and azimuthal angle (φ) of the velocity of the test particles striking the virtual detector. Polar angles of θ 90° ($\theta > 90°$) indicate northward (southward) particle motion, and azimuthal angle between $90° < \varphi < 270°$ ($\varphi < 90°$ or $\varphi > 270°$) indicate tailward (sunward) particle motion.

[19] There are two general trends to note from Figures 3a–3d. The first is that the IO fluxes are significantly lower than those from the high-altitude sources. This is especially true for the downtail direction, where the IO fluxes are always lower than the fluxes from the high-altitude sources in every flight direction. Over the north pole, the IO flux is just as high as that from the other sources (at directional number fluxes of 10^7 ions cm^{-2} s^- sr^{-1}), but it is limited to a single pixel in-flight direction, so the total flux at this location is dominated by the three high-altitude source processes. The second trend of Figure 3 is that the IO fluxes are more focused in-flight direction than those from the high-altitude sources. Usually, they extend over a portion of the flight directions covered by the high-altitude sources.

[20] Figure 4 shows energy spectra of omnidirectional differential number flux, averaged over flight direction, for the same locations and partitioned by source as in Figure 3. For a more direct comparison, the spectra for the sources are overlaid in the same panel. It is seen that the energy of the O^+ ions from the IO source are highly focused in energy at this radial distance. The value of that characteristic energy, however, changes with the location of the virtual detection. In the polar plume region, ionospheric outflow yields very high energy O^+ (over 10 keV), while in the central tail, this same source term yields very low energy O^+ (centered around 10 eV). In both places, the high-altitude sources give O^+ ions across a broad spectrum of energies. The high-altitude sources have two peaks, one at low energy (below 10 eV) and another at high energy (above 1 keV), with the flux ratio of these two relative maxima changing as a function of location.

3.2. Ion Escape Spatial Distributions

[21] Integrating the velocity space distributions yields a spatial pattern of the loss of particles to deep space. Figure 5 shows the escaping number flux of O^+ through the 4 R_M planet-centric shell for each of the source mechanisms (Figures 5a–5d) as well as the summation of all four sources (Figure 5e). While they all show the same basic features of a "polar plume" region, at high positive latitudes (i.e., near +90° latitude at all local times) in the direction of the solar wind convective electric field, connected to a central tail flow (around 0° latitude near midnight), there are certain distinguishing differences between the sources.

[22] A major difference among the spatial escape plots for each source mechanism is that the high-altitude ionization sources dominate the polar plume. The physical origin of the northern polar plume is primarily from the dayside

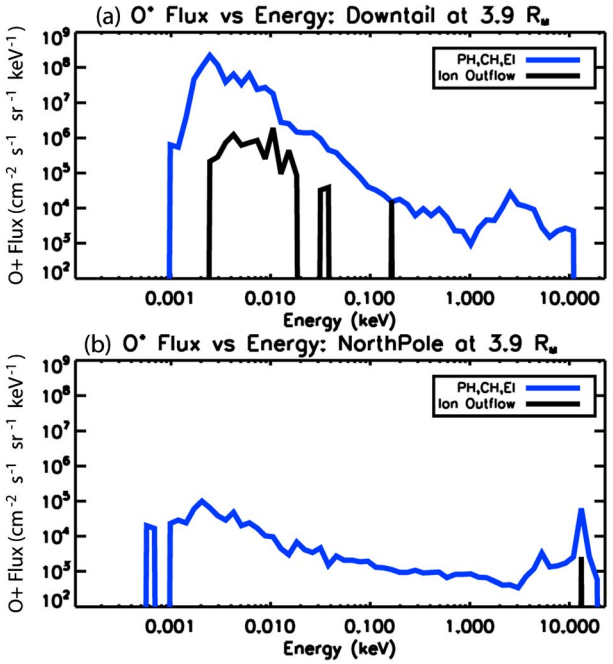

Figure 4. O^+ energy spectra, integrated over flight direction, at 3.9 R_M for (a) along the $-X_{MSE}$ axis (downtail) and (b) along the $+Z_{MSE}$ axis (over the North Pole). The blue curve is for the combined high-altitude source terms, and the black curve is for the IO source term.

northern hemispheric magnetosheath. The convective electric field that is associated with the reacceleration of the shocked solar wind accelerates these planetary pickup ions. O^+ has a much larger gyroradius than H^+ due to its mass and rather than being contained within the magnetosheath like the solar wind H^+, the pickup O^+ ions cross the bow shock and develop a high-energy beam-like velocity distribution (as seen in the previous section). The polar plume from ionospheric outflow is very narrow because the source is from the upflowing O^+ that crosses the magnetic pileup region into a region where they are affected by the large electric fields of the magnetosheath, which only happens at very high latitudes. Among the three high-altitude sources, the escaping fluxes from photoionization are a bit more structured than those from the other two processes, but in general, all three ionization mechanisms yield a similar spatial pattern.

[23] Another important difference for spatial escape is the central tail loss region, which contains most of the escaping IO particles. However, these particles still do not dominate at any particular spatial location. The IO source begins closer to the planet than the high-altitude source terms, by definition, and therefore creates a smaller, more focused, region of central tail loss. In this focused loss channel, the number flux from ionospheric outflow is comparable to that from high-altitude photoionization and larger than the fluxes from electron impact ionization or charge exchange.

[24] To further analyze this loss, Figure 6 shows the average energy of the escaping O^+ particles through the 4 R_M shell. As in Figure 5, the average energies are shown for each source process separately (Figures 6a–6d) and then for all of them together via a weighted average (Figure 6e), weighted proportionately to the number fluxes in Figure 5. The color scale is logarithmic with black indicating an average energy of 10 eV or less and red showing an average energy of tens of keV.

[25] Figure 6 illustrates that the energy of the escaping ionospheric outflow is notably different from that of the high-altitude sources. In particular, the polar plume is significantly hotter and the central tail loss region is cooler. The IO O^+ ions in the polar plume have an average energy around 10 keV, with some localized patches reaching 25 keV, while the IO ions in the central tail have an average energy below 100 eV. The average energies of the three high-altitude source terms are remarkably similar, with a polar plume average energy of ~7 keV and a central tail average energy of ~2 keV. The combined average energies in Figure 6e appear to closely resemble the high-altitude sources, reflecting the fact that the ionospheric outflow is a minor contributor to the escaping O^+ flux.

[26] A final feature of note in Figure 6 is the high-energy beam near the equator in the afternoon sector from the ionospheric outflow source term (Figure 6a). While the number flux of these escaping ions is only 10^4 $cm^{-2}\,s^{-1}$ (see Figure 5a), the average energy is over 10 keV. While it does not contribute significantly to the overall loss rate, it is an interesting packet of loss that should be investigated. Its origin is explained in section 4 below.

3.3. Total Escape Rate Comparison

[27] The final assessment to quantify the influence of ionospheric outflow on escape is with respect to the total O^+ loss. The results are provided in Table 1. The IO production rate is given in the second column, integrated over the entire 300 km altitude shell. This value can be compared with the $1.2 \times 10^{25}\,s^{-1}$ total production rate from the three high-altitude source processes. The total number of oxygen ions flowing through the inner boundary of the MTP simulation domain is over 50% larger than the total ionization rate in the MTP simulation domain.

[28] The loss of the ionospheric outflow O^+ particles through each of the MTP simulation boundaries was also calculated (inner and outer, respectively, in the third and fourth columns of Table 1). For comparison, the inner and outer boundary loss rates from the three high-altitude sources combined are $7.7 \times 10^{24}\,s^{-1}$ and $4.2 \times 10^{24}\,s^{-1}$, respectively. The loss through the inner boundary (i.e., bombardment of the Mars upper atmosphere) is dominated by the IO source, with a value over twice as large as that for the high-altitude sources. The situation is reversed for the outer boundary loss, with the high-altitude ionization processes contributing an order of magnitude more O^+ to the total escape rate.

[29] The IO escape rate percentage and efficiency (final two columns of Table 1) put these values into quantitative perspective. The IO escape percent (second to last column) is the IO escape rate divided by the total loss rate through the outer boundary, while the IO escape efficiency (last column) is the escape rate divided by the production rate. It is seen that, for this scenario with the MHD moments defining the outflow source conditions at 300 km altitude, ionospheric outflow contributes less than 10% to the total escape rate. Furthermore, even though the number of O^+ ions flowing into the MTP simulation domain through the lower boundary is larger than the ionization rate within the entire

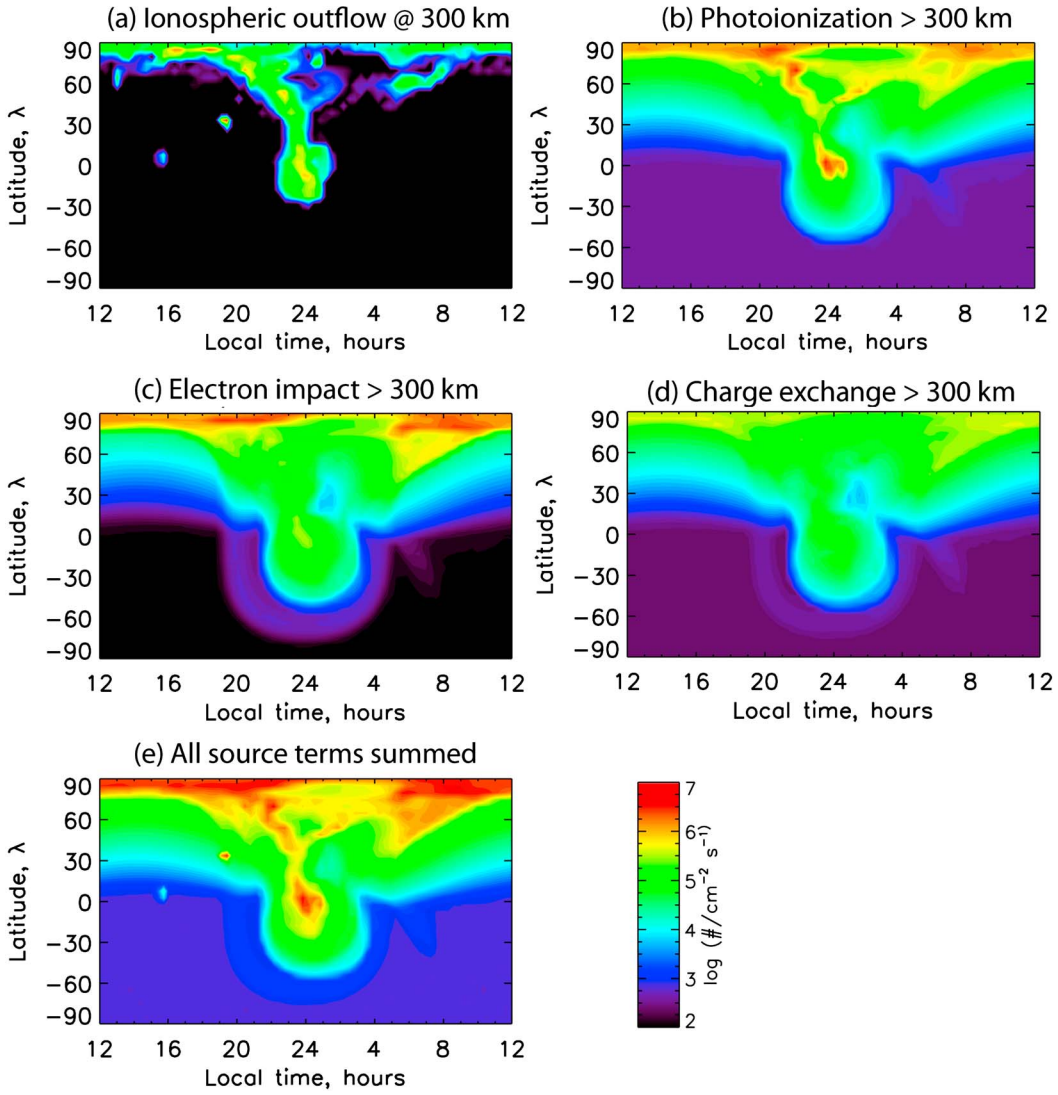

Figure 5. O^+ escape flux through a 4 R_M shell for (a–d) each source process and (e) a summation of all four source terms. Each plot has local time as the *x* axis (noon on the ends, midnight in the middle) and latitude as the *y* axis (over the poles at the top and bottom, over the equator in the middle), all on the same logarithmic color scale.

MTP simulation domain, only 2.4% of those incoming ions escape through the outer boundary.

3.4. Parametric Study of Ionospheric Outflow

[30] For the results shown above, the local MHD values at 300 km altitude were used to set the ionospheric outflow rate for initializing the MTP particles. It is useful to consider the influence of the outflow initialization on the results, in particular on the total escape rate of O^+ to deep space. The three MHD quantities used in the initialization are the O^+ density, velocity, and temperature. The following subsections examine the dependence of the loss rate on each of these parameters. While the background MHD simulation results are the same, the initialization quantities for the ionospheric outflow test particles are varied. While this means that the field through which these particles move is not consistent, the results elucidate the influence of these initialization parameters on the production and escape of ionospheric outflow.

3.4.1. Ionospheric Outflow Dependence on Initial Temperature

[31] Temperature is used for defining the ionospheric outflow by probabilistically setting the initial speed of the particle based on a Maxwellian distribution. Two additional parameters are used to assign a direction to this initial speed. As seen in Figure 1, the typical MHD ion temperature at 300 km altitude is around 1000 K, with dayside extrema between 100 and 10,000 K. For this parameter study, the temperature for the IO initialization was set to one of these three values everywhere on the shell: a low temperature of 100 K, an intermediate value of 1000 K, and a high case of 10,000 K. On the nightside, there is a region that rises to 10^6 K, but the bulk velocity, there is directed downward. Therefore, only the typical dayside temperatures were used in the parameter study.

[32] The results from these numerical experiments are shown in the first grouping of rows in Table 1. Because the production rate (second column) only depends on density

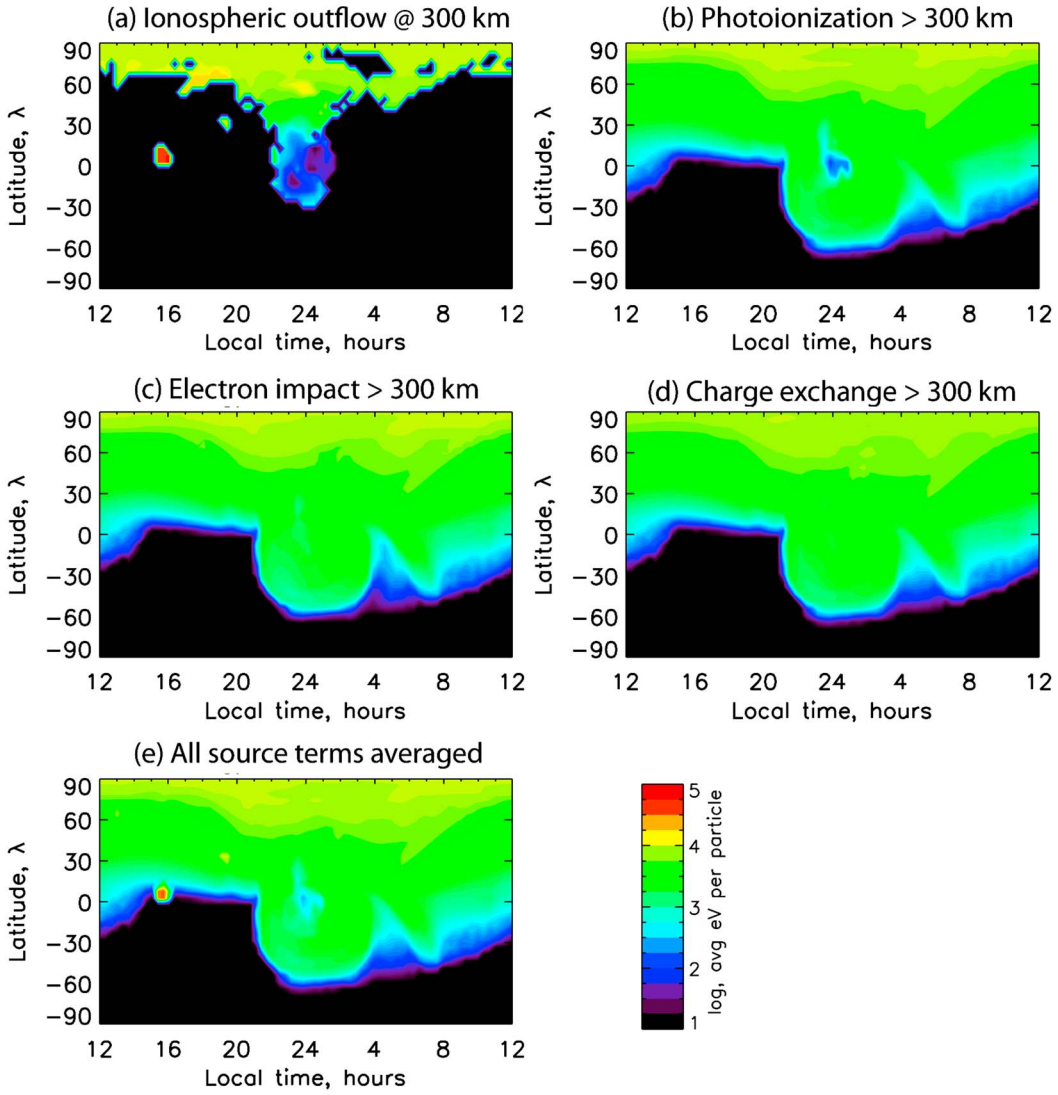

Figure 6. Average energies of the escaping O^+ through a 4 R_M shell for (a–d) each source process and (e) a weighted average of all four source terms. Each plot has local time as the x axis (noon on the ends, midnight in the middle) and latitude as the y axis (over the poles at the top and bottom, over the equator in the middle), all on the same logarithmic color scale.

and bulk velocity, this quantity does not change between these simulations. However, it is interesting that the inner and outer loss rates are essentially the same regardless of the temperature setting. There is a slight increase in the IO escape rate for the 10,000 K setting, but this rise is less than 10% from the baseline escape rate.

3.4.2. Ionospheric Outflow Dependence on Initial Velocity

[33] The dependence of ionospheric outflow of the initial drift velocity of the particles was also investigated. The drift velocity appears in two places in the initialization of the ionospheric outflow: first, it influences the weighting assigned to the particles because it is one of the two terms in the number flux calculation; second, it is used as an additive vector on the initial velocity for all of the IO particles in a source cell. These can be varied together or separately in the simulation. Varying only the number flux without changing the initial velocity is equivalent to changing the density, and this is discussed in the next subsection. Changing the initial velocity of the particles while keeping the total number flux the same is equivalent to changing not only the velocity but also the density inversely with the velocity. A third option is to keep the density constant and change the velocity both in the particle weighting calculation as well as in the initial condition.

[34] Let us consider these three options in reverse order. Results with the velocity changed in both places of the outflow initialization are given in the second section of Table 1. The production rate changes in direct proportion to the change in velocity, and on initial inspection, the loss through the inner and outer boundary also both increase with increasing initial velocity. The dependence of the loss is not the same as that for production, however, with more particles preferentially escaping through the outer boundary rather than striking the Mars upper atmosphere. This is evidenced in the IO escape efficiency (the last column), which increases

Table 1. Ionospheric Outflow as a Function of Initial Condition Parameters

Setting	IO Production (s^{-1})	IO Inner Loss (s^{-1})	IO Escape (s^{-1})	IO Escape Percent (% of total)	IO Escape Efficiency (% of IO Production)
MHD values	1.9×10^{25}	1.8×10^{25}	4.5×10^{23}	9.8	2.4
Changing temperature in velocity initialization					
$T = 10^2$ K	1.9×10^{25}	1.8×10^{25}	4.5×10^{23}	9.6	2.4
$T = 10^3$ K	1.9×10^{25}	1.8×10^{25}	4.5×10^{23}	9.7	2.4
$T = 10^4$ K	1.9×10^{25}	1.8×10^{25}	4.8×10^{23}	10.3	2.6
Changing bulk flow in both production rate and velocity initialization					
$U = 0.5$*local	9.3×10^{24}	9.0×10^{24}	2.3×10^{23}	5.2	2.5
$U = 2$*local	3.7×10^{25}	3.5×10^{25}	2.4×10^{24}	36	6.5
$U = 10$*local	1.9×10^{26}	1.4×10^{26}	4.1×10^{25}	91	22
Changing bulk flow in only the velocity initialization					
$U = 0.5$*local	1.9×10^{25}	1.8×10^{25}	4.5×10^{23}	9.7	2.4
$U = 2$*local	1.9×10^{25}	1.7×10^{25}	1.2×10^{24}	22	6.4
$U = 10$*local	1.9×10^{25}	1.4×10^{25}	4.1×10^{24}	50	22
Changing density in the production rate					
$n = 0.5$*local	9.3×10^{24}	9.0×10^{24}	2.3×10^{23}	5.1	2.4
$n = 2$*local	3.7×10^{25}	3.6×10^{25}	9.1×10^{23}	18	2.4
$n = 10$*local	1.9×10^{26}	1.8×10^{26}	4.5×10^{24}	52	2.4

with the initial velocity setting. In addition, for the case of an order of magnitude increase of the local MHD velocity, ionospheric outflow will dominate the total escape rate of O^+ to deep space.

[35] If the MHD flux used for calculating the IO production rate is kept constant, and only the particle initial bulk velocity is changed, then the results are a bit different (Table 1, third group of rows). Specifically, reducing the initial bulk velocity had essentially no effect on the results. Increasing the initial velocity of the particles, however, has a dramatic effect, with the escape rate approaching that of the high-altitude sources for an order of magnitude increase.

3.4.3. Ionospheric Outflow Dependence on Initial Density

[36] Results were also considered with a change in the density used for the IO initial conditions. The density only appears in the weighting factor given to the particles, a factor that is dependent on the MHD-calculated number flux through the 300 km altitude shell. If the velocity is allowed to vary inversely with the density in order to keep this flux constant, then density has no influence on the IO escape rates. However, if the velocity is kept at the MHD-defined value, then the IO production rate varies linearly with density. The last three rows of Table 1 list the loss values for ionospheric outflow when using different multiples of the local MHD density in the production rate calculation. The escape efficiency remains the same, but the relative contribution of IO to the total escape rate rises dramatically. When the local densities are increased by a factor of 10, ionospheric outflow dominates the total escape rate (52% of the total loss through the outer boundary). The escape efficiency is the same for the three density settings because the trajectories of the particles have not changed, only their weighting.

3.4.4. Ionospheric Outflow Dependence on Altitude of Insertion

[37] A final numerical experiment to consider is the dependence of the IO escape rate on the altitude at which the MHD fluxes are extracted (that is, the altitude of the ionospheric outflow source shell). All of the results to this point have been with the MHD results from 300 km altitude used for specifying particles in the first source cell of the MTP grid. Table 2 summarizes the results for a set of simulations in which the ionospheric outflow was specified and launched. The first column shows the altitude range of the MTP source grid where the IO particles were launched. The second column lists the total source rate for the IO process (summed over the shell), and the third column gives the relative size of this number with respect to the total source rate in the simulation (the source for the high-altitude pickup processes is 1.2×10^{25} s^{-1}). The fourth column lists the loss rate of IO particles through the inner boundary (at 300 km altitude), and the fifth column is the loss rate through the outer boundary (at 4 R_M planet-centric distance). The final two columns give the relative value of the IO escape rate with respect to the total escape rate (the outer boundary loss from the high-altitude sources is 4.5×10^{24} s^{-1}) and with respect to the IO source rate (the second column).

[38] It is seen that the IO source rate doubles as the source shell moves from 300 to ~400 km altitude. This can be due to one of two things: either the MHD flows have significantly turned outward from the planet, resulting in a substantial increase in outflow rate, or the ionization rate in this altitude

Table 2. Ionospheric Outflow as a Function of Launch Initialization Altitude

IO Altitude (km)	IO Production (s^{-1})	IO Production Percent (% of total)	IO Inner Loss (s^{-1})	IO Escape (s^{-1})	IO Escape Percent (% of total)	IO Escape Efficiency (% of IO Production)
300–337	1.9×10^{25}	60	1.8×10^{25}	4.5×10^{23}	9.8	2.4
337–374	3.0×10^{25}	71	2.2×10^{25}	8.2×10^{24}	66	27
374–412	3.9×10^{25}	76	2.1×10^{25}	1.8×10^{25}	81	46
412–450	3.9×10^{25}	76	1.7×10^{25}	2.2×10^{25}	84	57
450–488	3.5×10^{25}	74	1.1×10^{25}	2.4×10^{25}	85	69

Table 3. Solar Cycle Influence on the Relative Contribution of Ionospheric Outflow

Setting	IO Production (s^{-1})	IO Inner Loss (s^{-1})	IO Escape (s^{-1})	IO Escape Percent (% of total)	IO Escape Efficiency (% of IO Production)
Solar maximum	1.9×10^{25}	1.8×10^{25}	4.5×10^{23}	9.8	2.4
Solar minimum	2.0×10^{23}	7.8×10^{22}	1.2×10^{23}	27	61

range is still relatively large, dominating the actual outflow from the production below 300 km.

[39] There are also changes in the inner and outer boundary loss rate for ionospheric outflow as the source shell is elevated. The inner loss rate for the IO particles at first rises with source altitude, but then drops. This is expected because there are two competing processes: the IO source rate increases dramatically in this altitude range, but fewer particles hit the inner boundary as the initial altitude increases. The loss through the outer boundary, however, simply increases with rising source altitude, as expected. This yields a rise in escape efficiency from 2.4% to 69% across the range of IO source altitudes.

3.5. Solar Minimum Conditions

[40] All of the results presented above are for solar cycle maximum conditions in the MHD model and in the MTP production rates. For comparison, a similar numerical experiment was conducted from an analogous solar minimum MHD simulation, with identical upstream solar wind conditions but a different neutral atmosphere and photoionization rate. Again, the MHD parameters were extracted at 300 km altitude for use as the initialization values for the IO source in the MTP model.

[41] Table 3 presents the solar maximum and minimum results for total production and loss from ionospheric outflow.

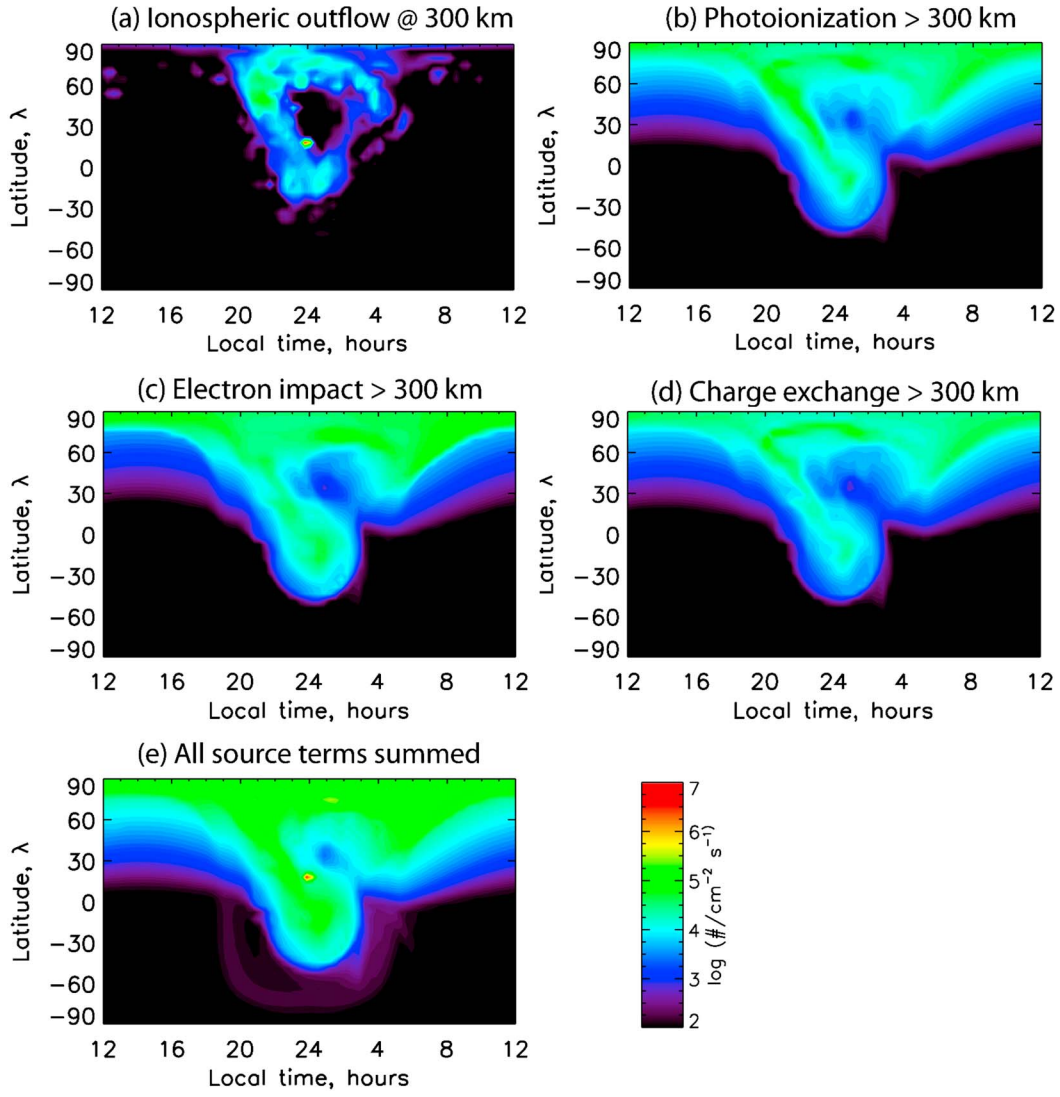

Figure 7. Spatial distributions of escaping O^+ number flux, like Figure 5, except for solar minimum instead of maximum conditions.

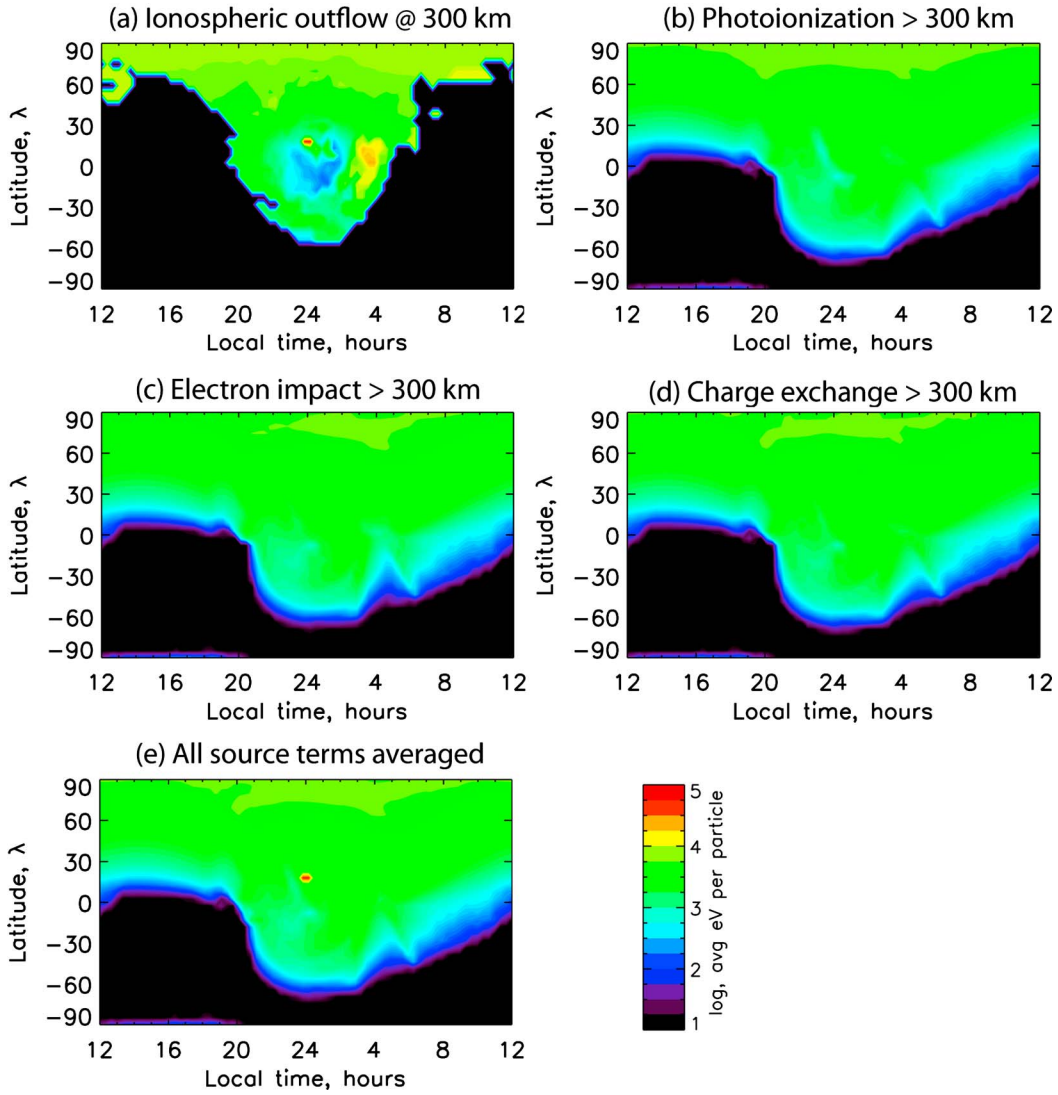

Figure 8. Spatial distributions of escaping O^+ average energy, like Figure 6, except for solar minimum instead of maximum conditions.

The IO production rate drops by two orders of magnitude between solar maximum and minimum. This is true for the high-altitude sources as well, which dropped by just over a factor of 10 to 9.9×10^{23} s^{-1} at solar minimum. So the IO source is now less than the high-altitude source of O^+ within the MTP simulation domain by nearly a factor of 5.

[42] The loss of the ionospheric outflow O^+ particles at solar minimum is quite different from that at solar maximum. In particular, the partitioning of the loss between the inner and outer boundaries is reversed between the two cycle phases, with solar minimum having a larger value of loss through the outer boundary (i.e., escape) than its inner boundary loss rate. The result is a rather different IO escape efficiency, changing from 2.4% at solar maximum to 61% at solar minimum. The contribution of ionospheric outflow to the total escape rate is also much bigger (nearly three times larger) at solar minimum than maximum. It is still less than half of the total, but at 27% of the total escape rate, it is now comparable to each of the other three source terms in the MTP (the escape efficiencies at solar minimum are 25%, 18%, and 30% for photoionization, charge exchange, and electron impact, respectively).

[43] Figure 7 shows the spatial distribution of the O^+ escape to deep space through a 4 R_M shell for the solar minimum simulation results. The fluxes are shown for each source term (Figures 7a–6d) as well as summation of all four sources (Figure 7e). The color scale is the same as that in Figure 5. Overall, the patterns are the same as that in Figure 5 with a polar plume in the $+Z_{MSE}$ direction that connects through one or more ribbons to the loss channel down the central tail. The flux values, however, are an order of magnitude or more lower.

[44] Similar to the solar maximum case, Figure 8 presents spatial distributions of the average energy of the escaping O^+ through a 4 R_M shell for solar minimum conditions. The plots for the high-altitude sources (Figures 8b–8d) and the weighted average energy plot (Figure 8e) closely resemble those for solar maximum values (compared with Figures 6b–6e), with the main difference being that the average energies are slightly lower in the solar minimum case.

The average energies for the IO source (Figure 8a) follow the same trend as those at solar maximum (compared with Figure 6a), but there is now a ring of keV-energy ions around the low-energy focused central tail. Some patches within this ring exceed 10 keV in average energy. Comparing this with the number flux loss distribution in Figure 7a, however, it is seen that these high-energy regions coincide with very low particle flux.

4. Discussion

[45] As seen in the results above, using the MHD output to define the ionospheric O^+ outflow rate at 300 km altitude yields high-altitude fluxes that are significantly smaller than those from the high-altitude sources (i.e., the ionization processes creating O^+ above 300 km altitude). The O^+ escape rate for ionospheric outflow was only 10% of the total loss rate to deep space, even though the production rate was 50% higher than that for the high-altitude sources. That is, the efficiency of escape is much lower for the IO source term than it is for the high-altitude source terms, to the point that ionospheric outflow is actually a small contributor to the total loss.

[46] There are several features of the IO velocity space distribution and spatial loss patterns that are worth discussing in further detail. The first is that, at high altitudes, the IO ions are more tightly focused in-flight direction than are the ions from the high-altitude sources. This is because the IO ions originate from a spatially limited location, whereas the high-altitude sources come from a large spatial region, essentially the entire near-Mars space environment, but in particular the dayside magnetosheath. This distributed source region for the high-altitude ionization processes yields a broader spectrum of O^+ flight directions in the tail.

[47] A related issue is the characteristic energy of the escaping IO ions. The first main feature to note regarding particle energy is that in the central tail, the IO ions are systematically lower in energy than those from the high-altitude sources. In order to reach the central tail, the IO ions remain close to the planet as they flow from the dayside to the nightside, staying below the region of large electric field in the magnetosheath where the solar wind is being reaccelerated. By avoiding this region and these large electric fields, the IO O^+ ions experience a smaller acceleration during their transport through near-Mars space and thus these ions remain at low energies, concentrated below 100 eV. Many of the high-altitude source particles, however, are created in the magnetosheath, instantly experiencing a large electric field and undergoing acceleration as they enter the central tail loss channel.

[48] A second point to make about the characteristic energy of the escaping IO ions is that, in the polar plume (that is, $+Z_{MSE}$, in the direction of the solar wind convective electric field), they are found at relatively higher energies than those ions from the high-altitude production mechanisms (by roughly a factor of two). There is a simple explanation for this reversal in characteristic energy between the two escape channel locations. For loss through the polar plume, IO ions must traverse the magnetic pileup boundary while still on the dayside of Mars (in the northern MSE hemisphere, as well). They are then exposed to the high electric fields of the magnetosheath and are accelerated outward from the planet (in the southern MSE hemisphere, this acceleration is back toward the planet, causing upper atmospheric bombardment). Such particles will cross through the entire magnetosheath, experiencing the full potential difference in this spatial region. The high-altitude source processes create ions throughout the magnetosheath and will consequently have a range of peak energies within the polar plume. Therefore, those IO particles that become part of the polar plume will have a systematically higher energy than those from the high-altitude sources.

[49] Figure 6 reveals the existence of a high-energy beam at 16 LT near 0° latitude from the ionospheric outflow source term (seen in Figures 6a and 6e). It is from a few test particles initiated near a region of strong crustal field in the Southern Hemisphere. These localized planetary magnetic fields distort the typical pattern of acceleration and transport for pickup ions, resulting in a rather different path toward escape for this particular group of particles. The average energy is so high because they have experienced the full energization through the magnetosheath but were directed toward a place on the outer boundary where there is no other flux from the ionospheric outflow source term (or from the other source terms). Figure 5 reveals that this packet of loss is not particularly high number flux, so it is not that significant in terms of the overall escape rate from Mars. However, it highlights the complexity that the crustal field regions interject into the standard scenario of ion loss from Mars.

[50] These source term-dependent features of the escaping O^+ velocity space and spatial pattern can be used for interpreting high-altitude observations from missions like Phobos-2, Mars Express, and the upcoming Mars atmosphere and volatile evolution satellite (in particular the plasma and fields instruments, especially the SupraThermal and Thermal Ion Composition sensor). Certain velocity space peaks are attributable to specific source processes, thus allowing for an analysis of the physical mechanisms of escape from high-altitude ion measurements.

[51] There was very little dependence of the IO escape rate on the initial temperature of the particles at 300 km altitude. This is because the average speed from these temperatures is well below the gravitational escape velocity at Mars. For the high temperature case, 10,000 K is still below 1 eV, which is less than half of the O^+ escape energy. So while the escape rate increased a small amount with increasing initial temperature, these simulations show that the contribution of ionospheric outflow does not depend on the temperature of the outflow (at least not within the temperature range explored here). This is similar to the findings of *Fang et al.* [2010b], who showed that the escape probability of pickup ions is not particularly sensitive to the initial temperature setting.

[52] When the initial velocity of the ionospheric outflow was varied, the escape rate of these particles was preferentially increased. This is not intuitive because the initial velocity could be pointed horizontally or downward, and therefore the expected result was that the efficiency should not change. It did change, though, because if the particle is directed downward, it will hit the inner boundary regardless of the initial velocity setting. Therefore, increasing the downward velocity of such particles did not increase the loss to the inner boundary. However, some particles directed upward could be redirected downward by gravity or electric

field forcing. An increase in upward velocity will act to overcome any downward force and help those particles escape. Therefore, it is actually natural to expect that an increase in the magnitude of the velocity, whatever its vector direction, will result in a preferential increase in the escape rate.

[53] Varying the density used to initialize the ionospheric outflow only changes the local upflowing number flux. This has the effect of changing the production rate but not the eventual trajectories of the test particles from this source term. Therefore, the escape efficiency is exactly the same for any setting of the initial density. However, the total production rate is directly proportional to this initial condition parameter, and therefore an increase of an order of magnitude in all of the local MHD density values yields an IO escape rate that is very similar to the total escape from the three high-altitude ionization processes.

[54] Taking all of the results in Table 1 together, it shows that ionospheric outflow could be a comparable or even dominant contributor to O^+ escape relative to the high-altitude sources, but only if the density or velocity of the upflowing ions is dramatically enhanced from that calculated by the MHD model. Temperature might have a similar influence as velocity, but the parameter regime explored in this study (which was the extrema of the MHD values) was not enough to have much of an influence on the escape of ionospheric outflow to deep space.

[55] The question arises as to how the density or bulk flow speed of the planetary ions could be significantly higher than the values calculated by the MHD model. The general answer is: processes not included in the MHD equation set. For instance, the MHD simulations were conducted with time-independent solar wind conditions and driven until a steady state solution was obtained. Therefore, any transient features caused by a changing solar wind dynamic pressure or IMF are not included in the background fields for the MTP calculations. These might include Kelvin-Helmholtz instabilities or reconnected magnetic plasmoids leading to temporary and localized increases in ionospheric outflow. *Brain et al*. [2010b] estimated this effect at perhaps 10% of the total escape ion escape rate at Mars. Another possibility is the presence of wave-particle interactions, preferentially heating and/or accelerating planetary ions in the topside ionosphere. Such terms are not included in the MHD results but could pose a substantial modification to the O^+ density or velocity near 300 km altitude. *Espley et al*. [2004] found ion cyclotron waves in the ionosphere, and *Ergun et al*. [2006] postulated that this could be a significant energy source for the planetary ions. Finally, parallel electric fields could also lead to significant O^+ energization at these altitudes. *Brain et al*. [2006] noted electron beams into the ionosphere, implying the presence of field-aligned electric potential differences, and *Lundin et al*. [2006a, 2006b] observed streaming planetary ions colocated with downward electron beams, indicating that such parallel electric fields are important for ion dynamics.

[56] A caveat to remember when considering the results of the IO parameter study is that, for these simulations, the source terms are intentionally set to different values than those used in the MHD model. That is, the same background electric and magnetic field is used for all of the MTP simulations, regardless of the IO settings. This inconsistency is an issue for all test particle simulations, of course; the motion of the particles could be different from that of the model supplying the background electric and magnetic fields, and this difference could lead to significant changes in density or weighted velocity and therefore a nonnegligible change in the electric and magnetic fields. The parameter study simulations conducted here add another inconsistency to the test particle results in that the particle source is also modified from that used to calculate the background fields. *Curry et al*. [2013a] addressed this for the MTP model and found that the species-weighted velocity, which enters into the magnetic induction equation in the MHD model, is very close to the MHD velocity everywhere except in two places: the polar plume and the central tail region. In the plume, the difference is small, with a velocity modification of ~10%. In the central tail, the difference can be large, but this is because the velocity is relatively small (as the velocity approaches zero, the ratio of the velocities dramatically increases). *Curry et al.* [2013b] illustrated electromagnetic field differences in the dayside sheath between solar maximum and solar minimum conditions. While the two solar cycle MHD results yielded different flight trajectories of sheath-origin pickup ions, the magnitude of the changes to the electric and magnetic fields were relatively minor. The changes to the ionospheric outflow initialization, especially when the velocity or density is increased by a factor of 10, could lead to substantial changes to the fields through which they are moving. While this means that the results are inconsistent, they are still valuable because they elucidate the general relationship between the fluid parameters near 300 km and the eventual escape of O^+ from Mars.

[57] The results for the simulations with ionospheric outflow defined at different altitude source shells (rather than at the inner boundary of the MTP code) showed that the IO production rate significantly increased as the source shell increased with altitude. This implies that there is an ionization source within the 300–400 km altitude range and defining the IO boundary condition above 300 km double counts this source term because production in this altitude range is also included in the high-altitude ionization mechanisms within the MTP. This altitude range is above the nominal ionosphere, which is typically defined to be coexistent with the thermosphere below the exobase. Therefore, production at these altitudes should be considered as part of the high-altitude source term rather than ionospheric outflow.

[58] A point of clarification is that the MTP inner boundary of 300 km is not necessarily the ionospheric boundary. For this study, however, all ions produced below the MTP inner boundary are given the label "ionospheric" and the flux through this inner boundary is labeled "ionospheric outflow." It should be noted that this is not a definition used in every study. *Ma et al*. [2004], the study from which the MHD results for the present study were taken, found that planetary ions dominate the charged particle density up to ~500 km at solar maximum and ~300 km at solar minimum (that is, this is the ion composition boundary, as determined from the simulation). They called this transition the upper boundary of the ionosphere. Others have called this transition the ion composition boundary, identified in both Phobos-2 and Mars Express measurements [e.g., *Breus et al*., 1991; *Sauer et al*., 1994; *Fränz et al*., 2006; *Boesswetter et al*., 2007]. These observational studies give a range for this transition, up to altitudes of 1000 km. This switch from planetary ion

dominance to solar wind ion dominance of the density does not have to coincide with the "top" of the ionosphere. At Earth, the ionosphere is often limited to same altitude range as the thermosphere (that is, up to the exobase). Even though planetary ions can dominate the density at much higher altitudes than this, the name given to the region is changed because the dominant physical processes are different. Specifically, names like plasmasphere, auroral outflow region, and polar wind are used for the geospace regions dominated by planetary ions above the ionosphere. A generic term for this boundary between planetary and solar wind density dominance is the geopause, coined by *Moore and Delcourt* [1995]. While there exists some ambiguity and even confusion in naming particles and regions of space, the definition used here is that the ionosphere is coincident with the thermosphere and therefore ends with the exobase.

[59] The solar minimum results were considerably different from those at solar maximum. The IO source increased in significance as a factor in ion escape, supplying a quarter of the total loss rate and therefore being comparable to each of the three high-altitude source processes as an originator of escaping O^+ ions. In addition, there were some notable differences in the spatial patterns of the escaping number flux and average energy of the IO particles at the 4 R_M shell. These differences can be explained by the change in the near-Mars electric field. A higher percentage of the IO source is allowed to penetrate through the magnetic pileup region and experience the large electric fields of the dayside magnetosheath. In the southern MSE hemisphere, such particles are subjected to this field and are accelerated northward into the central tail region, creating the halo of low flux but high-energy particles in Figures 7a and 8a. Note, however, that the inner boundary of the MTP simulation, and therefore the initialization altitude for ionospheric outflow, is the same for the solar maximum and minimum simulations. If the inner boundary is lowered for solar minimum to an altitude just above the exobase (say, for example, down to 250 or even 200 km), then the solar minimum IO escape efficiency might drop significantly. That is, this increased efficiency at solar minimum could be a function of initialization altitude. A full parameter study for the solar minimum input conditions was not included here for brevity, but the differences noted above make such a study an interesting one to explore in the future.

5. Conclusions

[60] Simulations were conducted of O^+ transport in the Mars space environment to investigate the relative contributions of ionospheric outflow to ion transport and escape. Using the combined results of an MHD model and a test particle code, high-altitude velocity space distributions and spatial patterns of escape were examined for both an IO source population (taken at 300 km altitude) and high-altitude source populations (from photoionization, charge exchange, and impact ionization above 300 km altitude).

[61] It was found that ionospheric outflow, as defined in our simulation configuration, is a rather small contributor to the total escape of O^+. High-altitude ionization processes significantly contribute to ion loss at Mars, providing 90% of the total O^+ loss, with O^+ leakage from below 300 km contributing an order of magnitude less. At high altitudes, ionospheric outflow is defined by several key features in velocity space, most notably a focused beam in-flight direction in a narrow region of space (compared to the high-altitude sources). The energy of ionospheric outflow changes dramatically depending on the pathway of escape; those that leave down the central tail are preferentially at low energies while those escaping via the polar plume are at relatively high energies.

[62] A series of MTP simulations were conducted that systematically varied the initial conditions for ionospheric outflow (keeping the high-altitude sources and the background fields the same). It was shown that ionospheric outflow can become significant, and even dominant, if the initialization density and/or velocity is substantially increased over the nominal MHD values extracted at 300 km. This implies that ionospheric outflow could be very important if processes not included in the MHD simulation are able to alter the O^+ characteristics in the topside ionosphere. For instance, this extra energization or density enhancement process could be wave-particle interactions, parallel electric fields, large-scale turbulence (i.e., Kelvin-Helmholtz oscillations), or solar wind-crustal field magnetic reconnection. These processes will preferentially influence the ionospheric outflow and escape rate relative to the high-altitude production processes, thus changing the proportion of the total loss that is attributable to lower-altitude ionization.

[63] Finally, solar minimum conditions were also explored and found to be similar to those at solar maximum in terms of the distribution and overall features of the O^+ lost to deep space. However, the escape efficiency dramatically increases at solar minimum, and ionospheric outflow can contribute a roughly equal portion to the total loss rate as each of the three high-altitude source terms.

[64] **Acknowledgments.** The authors thank NASA and NSF for supporting this work, particularly under NASA grants NNX07AN98G and NNX11AD80G, a NASA GSRP grant from Goddard Space Flight Center, and NSF grant AST-0908311.

[65] Masaki Fujimoto thanks the reviewers for their assistance in evaluating this paper.

References

Afonin, V., et al. (1989), Energetic ions in the close environment of Mars and particle shadowing by the planet, *Nature*, *341*, 616–618.

Andersson, L., R. E. Ergun, and A. I. F. Stewart (2010), The combined atmospheric photochemistry and ion tracing code: Reproducing the Viking lander results and initial outflow results, *Icarus*, *206*(1), 120–129.

Arkani-Hamed, J. (2001), A 50-degree spherical harmonic model of the magnetic field of Mars, *J. Geophys. Res.*, *106*, 23,197–23,208.

Arkani-Hamed, J. (2002), An improved 50-degree spherical harmonic model of the magnetic field of Mars derived from both high-latitude and low-latitude data, *J. Geophys. Res.*, *107*(E10), 5083, doi:10.1029/2001JE001835.

Barabash, S., A. Fedorov, R. Lundin, and J. Sauvaud (2007), Martian atmospheric erosion rates, *Science*, *315*, 501–503.

Boesswetter, A., T. Bagdonat, U. Motschmann, and K. Sauer (2004), Plasma boundaries at Mars: A 3-D simulation study, *Ann. Geophys.*, *22*, 4363–4379, doi:10.0576/ag/2004-22-4363.

Boesswetter, A., et al. (2007), Comparison of data from ASPERA-3/Mars-Express with a 3-D hybrid simulation, *Ann. Geophys.*, *25*, 1851–1864.

Bougher, S. W., S. Engel, R. G. Roble, and B. Foster (2000), Comparative terrestrial planet thermosphere: 3. Solar cycle variation of global structure and winds at solstices, *J. Geophys. Res.*, *105*, 17,669–17,692.

Brain, D. A., J. S. Halekas, L. M. Peticolas, R. P. Lin, J. G. Luhmann, D. L. Mitchell, G. T. Delory, M. H. Acuna, and H. Reme (2006), On the origin of aurorae at Mars, *Geophys. Res. Lett.*, *33*, L01201, doi:10.1029/2005GL024782.

Brain, D., et al. (2010a), A comparison of global models for the solar wind interaction with Mars, *Icarus*, *206*(1), 139–151.

Brain, D. A., A. H. Baker, J. Briggs, J. P. Eastwood, J. S. Halekas, and T.-D. Phan (2010b), Episodic detachment of Martian crustal magnetic fields leading to bulk atmospheric plasma escape, *Geophys. Res. Lett.*, *37*, L14108, doi:10.1029/ 2010GL043916.

Brecht, S. H. (1997), Hybrid simulations of the magnetic topology of Mars, *J. Geophys. Res.*, *102*, 4743–4750.

Brecht, S. H., and S. A. Ledvina (2006), The solar wind interaction with the Martian ionosphere/atmosphere, *Space Sci. Rev.*, *126*(1–4), 15–38.

Brecht, S. H., and S. A. Ledvina (2010), The loss of water from Mars: Numerical results and challenges, *Icarus*, *205*, 164–173.

Brecht, S. H., and S. A. Ledvina (2012), Control of ion loss from Mars during solar minimum, *Earth Planets Space*, *64*, 165–178.

Breus, T. K., et al. (1991), The solar wind interaction with Mars: Consideration of Phobos-2 mission observations of an ion composition boundary on the dayside, *J. Geophys. Res.*, *96*, 11,165–11,174.

Carlsson, E., et al. (2006), Ion composition of the escaping plasma at Mars, *Icarus*, *182*, 320–328.

Cravens, T. E., J. U. Kozyra, A. Nagy, T. Gombosi, and M. Kurtz (1987), Electron impact ionization in the vicinity of comets, *J. Geophys. Res.*, *92*, 7341–7353.

Cravens, T. E., A. Hoppe, S. A. Ledvina, and S. McKenna-Lawlor (2002), Pickup ions near Mars associated with escaping oxygen atoms, *J. Geophys. Res.*, *107*(A8), 1170, doi:10.1029/2001JA000125.

Curry, S. M., M. W. Liemohn, X. Fang, Y. Ma, A. F. Nagy, and J. Espley (2013a), The influence of production mechanisms on pickup ion loss at Mars, *J. Geophys. Res. Space Physics*, *118*, 554–569, doi:10.1029/ 2012JA017665.

Curry, S. M., M. Liemohn, X. Fang, D. Brain, and Y. Ma (2013b), Simulated kinetic effects of the corona and solar cycle on high altitude ion transport at Mars, *J. Geophys. Res. Space Physics*, *118*, doi:10.1002/jgra.50358, in press.

Dubinin, E., M. Fraenz, J. Woch, S. Barabash, and R. Lundin (2009), Long-lived auroral structures and atmospheric losses through auroral flux tubes on Mars, *Geophys. Res. Lett.*, *36*, L08108, doi:10.1029/ 2009GL038209.

Eastwood, J. P., D. A. Brain, J. S. Halekas, J. F. Drake, T. D. Phan, M. Øieroset, D. L. Mitchell, R. P. Lin, and M. Acuna (2008), Evidence for collisionless magnetic reconnection at Mars, *Geophys. Res. Lett.*, *35*, L02106, doi:10.1029/2007GL032289.

Ergun, R. E., L. Andersson, W. K. Peterson, D. Brain, G. T. Delory, D. L. Mitchell, R. P. Lin, and A. W. Yau (2006), Role of plasma waves in Mars' atmospheric loss, *Geophys. Res. Lett.*, *33*, L14103, doi:10.1029/ 2006GL025785.

Espley, J. R., P. A. Cloutier, D. A. Brain, D. H. Crider, and M. H. Acuña (2004), Observations of low-frequency magnetic oscillations in the Martian magnetosheath, magnetic pileup region, and tail, *J. Geophys. Res.*, *109*, A07213, doi:10.1029/2003JA010193.

Fang, X., M. W. Liemohn, A. F. Nagy, Y. Ma, D. L. De Zeeuw, J. U. Kozyra, and T. Zurbuchen (2008), Pickup oxygen ion distribution around Mars, *J. Geophys. Res.*, *113*, A02210, doi:10.1029/2007JA012736.

Fang, X., M. W. Liemohn, A. F. Nagy, J. G. Luhmann, and Y. Ma (2010a), On the effect of the Martian crustal magnetic field on atmospheric erosion, *Icarus*, *206*, 130–138, doi:10.1016/j.icarus.2009.01.012.

Fang, X., M. W. Liemohn, A. F. Nagy, J. G. Luhmann, and Y. Ma (2010b), Escape probability of Martian atmospheric ions: Controlling effects of the electromagnetic fields, *J. Geophys. Res.*, *115*, A04308, doi:10.1029/ 2009ja14929.

Fang, X., S. W. Bougher, R. E. Johnson, J. G. Luhmann, Y. Ma, Y.-C. Wang, and M. W. Liemohn (2013), The importance of pickup oxygen ion precipitation to the Mars upper atmosphere under extreme solar wind conditions, *Geophys. Res. Lett.*, doi:10.1002/grl.50415, in press.

Fedorov, A., et al. (2006), Structure of the Martian wake, *Icarus*, *182*, 329–336.

Fränz, M., et al. (2006), Plasma moments in the environment of Mars, *Space Sci. Rev.*, *126*, 165–207, doi:10.1007/s11214-006-9115-9.

Harnett, E. M. (2009), High-resolution multifluid simulations of flux ropes in the Martian magnetosphere, *J. Geophys. Res.*, *114*, A01208, doi:10.1029/ 2008JA013648.

Harnett, E. M., and R. M. Winglee (2006), Three-dimensional multifluid simulations of ionospheric loss at Mars from nominal solar wind conditions to magnetic cloud events, *J. Geophys. Res.*, *111*, A09213, doi:10.1029/2006JA011724.

Johnson, R. E. (1994), Plasma-induced sputtering of an atmosphere, *Space Sci. Rev.*, *69*, 215–253.

Kallio, E., and P. Janhunen (2002), Ion escape from Mars in a quasi-neutral hybrid model, *J. Geophys. Res.*, *107*(A3), 1035, doi:10.1029/ 2001JA000090.

Kallio, E., and H. Koskinen (1999), A test particle simulation of the motion of oxygen ions and solar wind protons near Mars, *J. Geophys. Res.*, *104*, 557–579.

Kallio, E., H. Koskinen, S. Barabash, R. Lundin, O. Norberg, and J. G. Luhmann (1994), Proton flow in the Martian magnetosheath, *J. Geophys. Res.*, *99*, 23,547–23,599.

Kallio, E., K. Liu, R. Jarvinen, V. Pohjola, and P. Janhunen (2010), Oxygen ion escape at Mars in a hybrid model: High energy and low energy ions, *Icarus*, *206*(1), 152–163.

Kirsch, E., et al. (1991), Pickup ions ($E\ O^+ > 55$ keV) measured near Mars by Phobos-2 in February/March 1989, *Ann. Geophys.*, *9*, 761–767.

Li, L., and Y. Zhang (2009), Model investigation of the influence of the crustal magnetic field on the oxygen ion distribution in the near Martian tail, *J. Geophys. Res.*, *114*, A06215, doi:10.1029/2008JA013850.

Liemohn, M. W., Y. Ma, R. A. Frahm, X. Fang, J. U. Kozyra, A. F. Nagy, J. D. Winningham, J. R. Sharber, S. Barabash, and R. Lundin (2006), Mars global MHD predictions of magnetic connectivity between the dayside ionosphere and the magnetospheric flanks, *Space Sci. Rev.*, *126*, 63–76.

Liemohn, M. W., Y. Ma, A. F. Nagy, J. U. Kozyra, J. D. Winningham, R. A. Frahm, J. S. Sharber, S. Barabash, and R. Lundin (2007), Numerical modeling of the magnetic topology near Mars auroral observations, *Geophys. Res. Lett.*, *34*, L24202, doi:10.1029/2007GL031806.

Luhmann, J. G. (1990), A model of the ion wake of Mars, *Geophys. Res. Lett.*, *17*, 869–872.

Luhmann, J. G., and J. U. Kozyra (1991), Dayside pick-up oxygen ion precipitation at Venus and Mars: Spatial distributions, energy deposition, and consequences, *J. Geophys. Res.*, *96*, 5457–5467.

Lundin, R., et al. (1989), First measurements of the ionospheric plasma escape from Mars, *Nature*, *341*(6243), 609–612.

Lundin, R., A. Zakharov, R. Pellinen, S. W. Barabasj, H. Borg, E. M. Dubinin, B. Hultqvist, H. Koskinen, I. Liede, and N. Pissarenko (1990), ASPERA/Phobos measurements of the ion outflow from the Martian ionosphere, *Geophys. Res. Lett.*, *17*, 873–876.

Lundin, R., et al. (2004), Solar wind-induced atmospheric erosion at Mars: First results from ASPERA-3 on Mars Express, *Science*, *305*, 1933–1936.

Lundin, R., et al. (2006a), Plasma acceleration above Martian magnetic anomalies, *Science*, *311*, 980–983.

Lundin, R., et al. (2006b), Ionospheric plasma acceleration at Mars: ASPERA-3 results, *Icarus*, *182*, 308–319.

Lundin, R., S. Barabash, A. Fedorov, M. Holmstrom, H. Nilsson, J.-A. Sauvaud, and M. Yamauchi (2008), Solar forcing and planetary ion escape from Mars, *Geophys. Res. Lett.*, *35*, L09203, doi:10.1029/ 2007GL032884.

Lundin, R., S. Barabash, M. Holmstrom, H. Nilsson, M. Yamauchi, E. M. Dubinin, and M. Fraenz (2009), Atmospheric origin of cold ion escape from mars, *Geophys. Res. Lett.*, *36*, L17202, doi:10.1029/ 2009GL039341.

Ma, Y., A. F. Nagy, I. V. Sokolov, and K. C. Hansen (2004), Three-dimensional, multispecies, high spatial resolution MHD studies of the solar wind interaction with Mars, *J. Geophys. Res.*, *109*, A07211, doi:10.1029/2003JA010367.

McKenna-Lawler, S., E. Kallio, R. Jarvinen, and V. Afonin (2012), Magnetic shadowing of high energy ions at Mars and how this effect can be simulated using a hybrid model, *Earth Planets Space*, *64*(2), 247–256.

McKenna-Lawlor, S. M. P., V. Afonin, Y. Yeroshenko, E. Keppler, E. Kirsch, and K. Schwingenschuh (1993), First identification in energetic particles of characteristic plasma boundaries at Mars and an account of various energetic particle populations close to the planet, *Planet. Space Sci.*, *41*, 373–380.

Modolo, R., G. M. Chanteur, E. Dubinin, and A. P. Matthews (2005), Influence of the solar EUV flux on the Martian plasma environment, *Ann. Geophys.*, *23*, 433–444.

Moore, T. E., and D. C. Delcourt (1995), The geopause, *Rev. Geophys.*, *33*, 175–209.

Penz, T., N. V. Erkaev, H. K. Biernat, and H. Lammer (2004), Ion loss on Mars caused by the Kelvin-Helmholtz instability, *Planet. Space Sci.*, *52*, 1157–1167, doi:10.1016/j.pss.2004.06.001.

Perez-de-Tejada, H., R. Lundin, H. Durand-Manterola, and M. Reyes-Ruiz (2009), Solar wind erosion of the polar regions of the Mars ionosphere, *J. Geophys. Res.*, *114*, A02106, doi:10.1029/2008JA013295.

Sauer, K., A. Bogdanov, and K. Baumgärtel (1994), Evidence of an ion composition boundary (protonopause) in bi-ion fluid simulations of solar wind mass loading, *Geophys. Res. Lett.*, *21*, 2255–2258.

Verigin, M. I., et al. (1991), Ions of planetary origin in the Martian magnetosphere (Phobos-2/Taus experiment), *Planet. Space Sci.*, *39*, 131–137.